TÜBİTAK

Turk J Agric For
33 (2009) 155-163
© TÜBİTAK
doi:10.3906/tar-0807-13

Observation of Liquid Permeability Related to Anatomical Characteristics in *Samanea saman*

Sheikh Ali AHMED, Su Kyoung CHUN*

Department of Wood Science and Engineering, College of Forest and Environmental Sciences,
Kangwon National University, Chunchon 200-701, Republic of KOREA

Received: 14.07.2008

Abstract: This paper examines wood anatomy as it relates to safranine solution penetration in *Samanea saman*, which belongs to the family Mimosoideae and is native to Bangladesh. The wood of this species was characterized by diffuse-porous vessels with simple perforations, alternate and opposite vestured intervessel pits, gums in heartwood vessels, vascicentric paratracheal axial parenchyma, lozenge-aliform, confluent prismatic crystals in fiber, and chambered axial parenchyma cells. Different anatomical features affect longitudinal and lateral liquid permeability. Herein microstructures that controlled liquid penetration are described and compared. We observed that ray cell lumen diameter, end-wall pit number and diameter, ray cell length, vessel number, and both vessel and fiber diameter and length affected the depth of liquid flow. Safranine solution formed a meniscus while traveling through different types of cells. Air trapped in capillaries blocked safranine solution penetration. Following a go-stop-go cycle, the speed of penetration slowly decreased over time.

Key Words: Wood anatomy, hardwood, safranine solution, meniscus, capillary phenomenon

Introduction

As the structure of vessels facilitates longitudinal liquid flow in living trees, it is not surprising that vessels play a primary role in liquid penetrability. Nonetheless, their effectiveness is dependent upon size, number, and distribution, and even more importantly upon the extent of extraneous materials and tyloses present, as well as upon the character of pitting that leads to contiguous cells. The factors emphasized in the present study are vessel anatomical features, and fiber and ray parenchyma related to liquid permeability. According to Watanabe et al. (1998), there are 2 types of liquid movement in wood: diffusion through the cell walls and flow in the cell lumens. The latter is considerably more prevalent during wood processing. The wetting rate via capillary action is much faster than via diffusion; therefore, the present study aimed to observe free liquid soaking via capillary action only. This liquid flow not only depends on the moisture content of wood (Hansmann et al., 2002), but also on the principle direction of the grain (Bolton, 1988; Fujii et al., 2001; Kamke and Lee, 2007), as well as various physical, chemical (Hansmann et al., 2002), and anatomical characteristics (Thomas, 1976; Owoyemi and Kayode, 2008).

Although fiber often constitutes the majority of woody tissue, general fiber is not considered as important as vessels in primary liquid flow (Leal et al., 2007). Nonetheless, fiber permeability may influence the subsequent spreading of liquid from vessels or other cells connecting them to pits. Compared to vessels, non-perforated fibers are thick walled and have relatively small pits that are not adapted for efficient liquid

* Correspondence to: chun@kangwon.ac.kr

conduction. In addition, interconnecting pits provide one of the main pathways for the flow of liquid between cells, and their structure and distribution affects the penetration of liquid in wood (Sano, 2004). In addition, the air that is compressed during liquid penetration lowers the permeability of wood (Virta et al., 2006). In this regard Banks (1981) reported that air is compressed during water soaking and additional counter pressure is formed that substantially reduces permeability.

The present study was primarily concerned with finding an explanation for treatability differences in different cells and to determine the cause of that variability as it relates to anatomical features. A considerable quantity of anatomical data are available for *Samanea*; however, only a limited number of attempts have been made to understand the behavior of liquid penetration related to anatomical structure. Therefore, an important tropical wood species, *Samanea saman*, was studied in an effort to determine the anatomical features that affect non-steady liquid (safranine solution) flow in radial and longitudinal directions.

Materials and Methods

Wood Identification

Wood discs (50 mm long) were made from freshly cut logs of *Samanea saman* (Jacq.) Merr., with their bark still attached from 2 m above ground level. The 20-year-old specimen was collected from Dhaka, Bangladesh (23°51′N, 90°24′E). Discs were then air-dried in the laboratory. From the air-dried discs, pieces of wood were separated, including sapwood and heartwood, and converted as shown in Figure 1. Microscopic slides and macerations were made according to standard techniques (Baas and Zhang, 1986). To confirm the deposits in the vessels, microtomed sections were stained with iodine and chrysoidin. This staining method, which has been proven to permanently stain starch in tree tissue, facilitated microscopic observation (Essiamah and Eschrich, 1985). The sections were stained with chrysoidin (1% chrysoidin in 70% ethyl alcohol) solution for 5 min and then were counterstained with Lugol's solution for 7 min. The stained samples were mounted with euparal for microscopic observation. Samples for FESEM (field emission scanning electron microscope) observation were prepared according to Exley et al. (1977). At different resolutions and magnifications the wood was then examined at the accelerating voltage of 15 kV in a Hitachi S-4300 FESEM. Different microscopic measurements were made for 2 diffuse porous wood species, viz. *Populus tomentiglandulosa* T. Lee and *Gmelina arborea* Roxb. These measurements were made in order to determine which anatomical and microstructural features might be responsible for the variation in liquid penetration. The permeability of these 2 species was

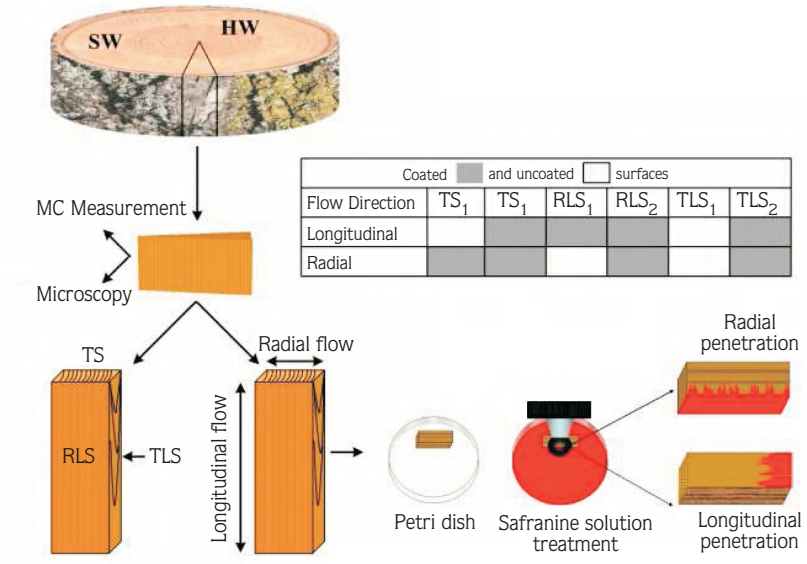

Figure 1. Collection and preparation of the experimental samples. SW: Sapwood; HW: heartwood; TS: transverse section; RLS: radial-longitudinal section; TLS: tangential-longitudinal section.

reported by Ahmed and Chun (2007), Choi et al. (2007), and Ahmed et al. (2007). In all, 100 measurements of various micro-structural features were made. The terminology used herein and the method used to determine quantitative features conform to the recommendations of the IAWA Feature List (IAWA Committee, 1989).

Block Preparation

Two 50 × 50-mm stakes were taken from outer sapwood and heartwood, and each was cut into 3 specimens (producing 6 specimens each 50 mm long), which were then further divided along their length into 3 blocks–a 5-mm block for moisture content measurement, a 40-mm block for treatment, and another 5-mm block microscopic examination. For safranine treatment the exact air dried sample size was maintained at 40 mm (longitudinal) × 10 mm (radial) × 5 mm (tangential). Samples for treatment were sealed with silicon resin, leaving their ends or radial faces open, allowing either longitudinal or radial flow (Figure 1). This was done to prevent leakage onto other surfaces.

Preparation of Safranine Solution (1%)

Into a 1-l volumetric flask, 10 g of safranine powder (Junsei Chemical Co., Ltd.) was placed and 500 ml of 50% ethyl alcohol was added. After mixing properly, distilled water was added to bring the volume to 1 l. Safranine solution was used because of its bright color and it facilitates observation of the penetration path in different cells.

Measurement of Surface Tension of Safranine Solution

If a liquid has a contact angle, θ, with a thin tube it produces an associated vertical force on the liquid, the capillary force of which is given by:

$$2\pi r\gamma Cos(\theta) \quad (1)$$

where r is the radius of the capillary (cm) and γ is the surface tension (dynes cm^{-1}). If the wetting angle, θ, is < 90°, the liquid will rise in a thin tube, whereas if the angle is > 90°, the liquid in the capillary will drop. This is due to the surface energy between the liquid and the walls of the capillary. If this energy is favorable, the liquid wants to increase its contact with the capillary surfaces, which induces the liquid to rise in the capillary tube. The height to which a liquid rises or falls is determined by a balance between the capillary force and the force of gravity, $\pi r^2 h\rho g$. When the liquid is in a stable condition (neither rising nor receding), these 2 forces are equal; so:

$$\gamma(2\pi r) = \rho h(\pi r^2)g \quad (2)$$

where ρ is density (g cm^{-3}), g is gravity acceleration (980.665 cm s^{-2}), and h is height (cm) of the capillary. From equation (2) we can obtain the surface tension:

$$\gamma = {}^1/_2(\rho ghr) \quad (3)$$

Surface tension of the safranine solution was measured with the capillary rise method, using equation (3) at 24 °C. The unit was expressed in dynes cm^{-1}.

Observation of Liquid Impregnation

Safranine solution penetration behavior was observed with an *i*-Camscope (model SV32). While observing safranine solution penetration, the room temperature was 24 °C and the wind speed was 0 m s^{-1}. The coated sample was fixed on a petri dish and the safranine solution was poured onto it. Using the *i*-Solution v.2.5 image processing program, a 5-min safranine solution impregnation video file was captured, which contained 300 frames. Specific digital images at 1, 2, 3, 4, and 5 min were selected from the captured video frames with VitrualDub v.1.6.16 software. Then, penetration depth was measured in millimeters from the digital images with the *i*-Solution program. Three replications were conducted to measure penetration depth and for each replication, 7 measurements were made.

Results

Wood anatomical features

Anatomical features observed in this species included indistinct growth ring boundaries marked by marginal parenchyma, and vessels arranged in a diffuse-porous pattern (Figure 2). The vessels had simple perforation plates (Figure 3), vessel-ray pits had distinct borders, similar to intervessel pits (Figure 4), and non-septate fiber was observed with simple to minutely bordered pits (Figure 5). Mean fiber length was 707.96 ± 149.66 µm (range: 420.20-1080.00 µm). Tangential vessel lumina diameter was 145.24 ± 38.87 µm (range: 74.29-225.85 µm). Axial parenchyma was banded and seemingly marginal, apotracheal axial parenchyma was diffuse (Figure 6), paratracheal axial parenchyma was vasicentric, confluent, and lozenge-aliform. Cells per axial parenchyma strand ranged between 2 and 8, but 8

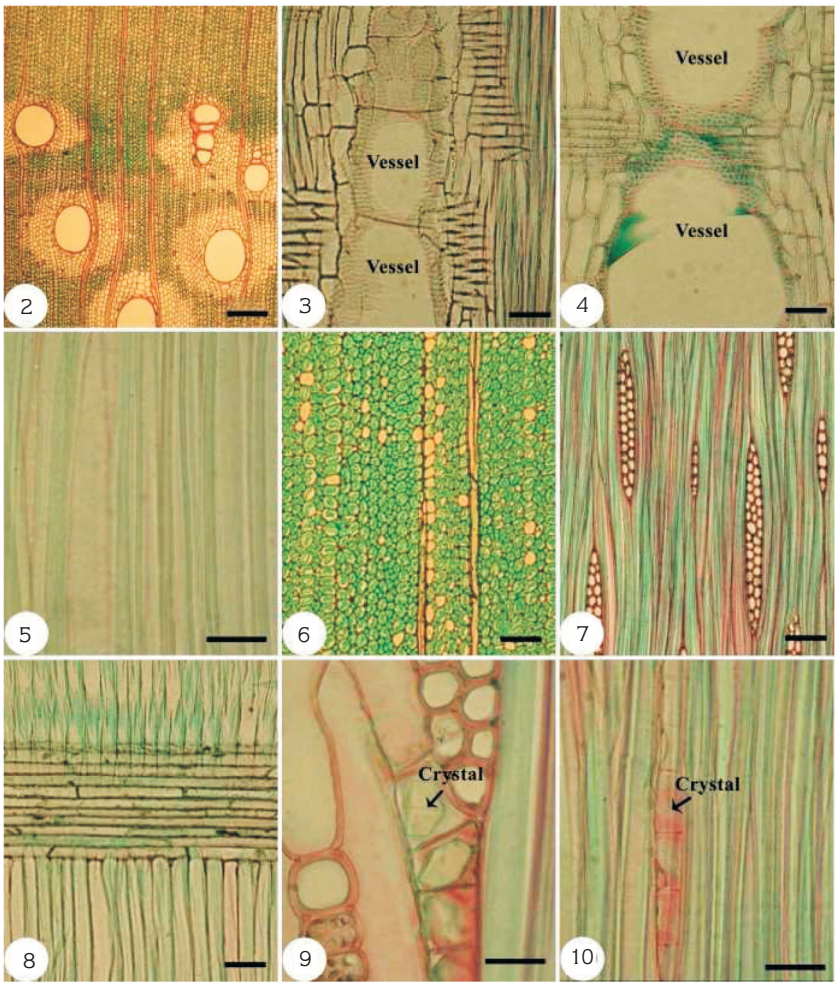

Figures 2-10. Optical microphotographs. 2: Distinct growth ring boundaries, wood ring-porous, axial parenchyma in marginal bands, and axial parenchyma, confluent. 3: Simple perforation plate. 4: Vessel-ray pit. 5: Non-septate fiber. 6: Axial parenchyma, diffuse. 7: Ray width, 1-3 ray cells. 8: All procumbent rays. 9: Prismatic crystals in chambered axial parenchyma. 10: Prismatic crystals in fiber. Scale bar in 1 and 5 = 200 µm; in 2, 3, 6, and 7 = 50 µm; in 4, 8, and 9 = 20 µm.

cells was more common, with 2-9 mostly biseriate rays per mm (Figure 7). All ray cells were procumbent (Figure 8). Prismatic crystals were observed in chambered axial parenchyma (Figure 9) and fibers (Figure 10). Intervessel pits were alternate (Figure 11), occasionally opposite (Figure 12), and vestured (Figure 13). Deposits were observed in the vessels (Figure 14). Fiber was thin to thick walled (Figure 15) and axial parenchyma was in strands (Figure 16).

This is a commercially important wood species. The basic specific gravity of this species is medium (0.40-0.75). The heartwood was brown and sapwood was light brown. It had no distinctive odor. The water extract was various shades of red and the ethanol extract was colorless. Froth test results were positive and chrome azurol-S test results were negative. The splinter burned to a full ash, which was white.

Safranine Solution Penetration Observed with an i-Camscope

As can be seen in Figure 17, it is clear that penetration in sapwood was higher than in heartwood. Sapwood was

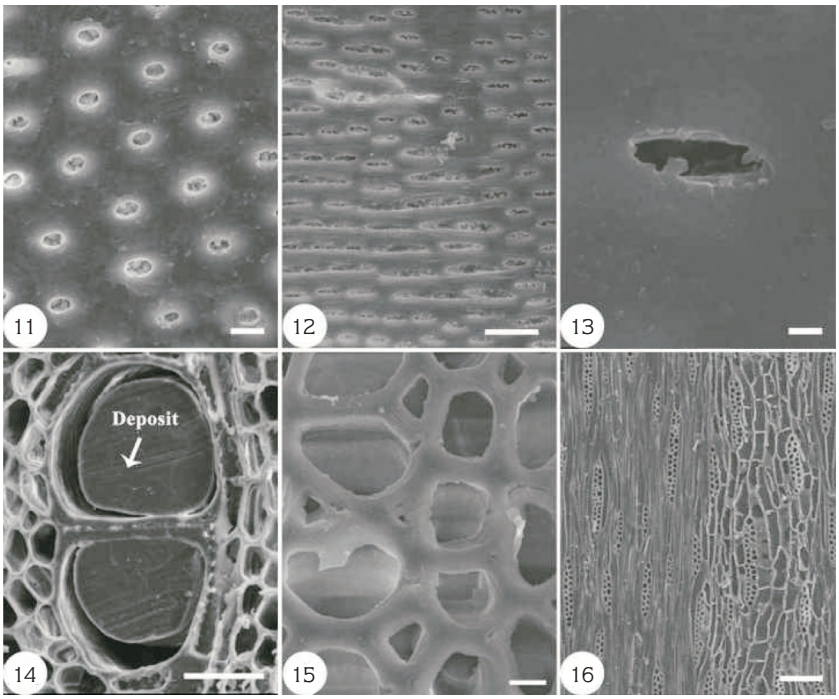

Figures 11-16. FE-SEM photographs. 11: Alternate intervessel pit. 12: Opposite intervessel pit. 13: Vestured pit. 14: Deposit in vessel. 15: Thin to thick walled fibers. 16: Two-eight cells per parenchyma strand. Scale bar in 10 and 14 = 4 µm; in 11 = 15 µm; in 12 = 1 µm; in 13 = 50 µm; in 15 = 5 µm.

1.57 times more permeable in the radial direction (measured at 5 min) and 2.24 times more permeable in the longitudinal direction (measured at 5 min) than heartwood; however, longitudinal penetration depth was about 232% greater than radial penetration. In both the radial and longitudinal directions, permeability decreased as flow path length increased. Additionally, after 1 min safranine solution penetration depth decreased up to 77% at 2 min, 90% at 3 min, 94% at 4 min, and 95% at 5 min in the radial direction, whereas it decreased up to 85% at 2 min, 89% at 3 min, 94% at 4 min, and 94% at 5 min.

Discussion

The permeability of some wood species decreases with increased moisture content (Comstock, 1968). In addition, excess moisture in wood voids may act as a

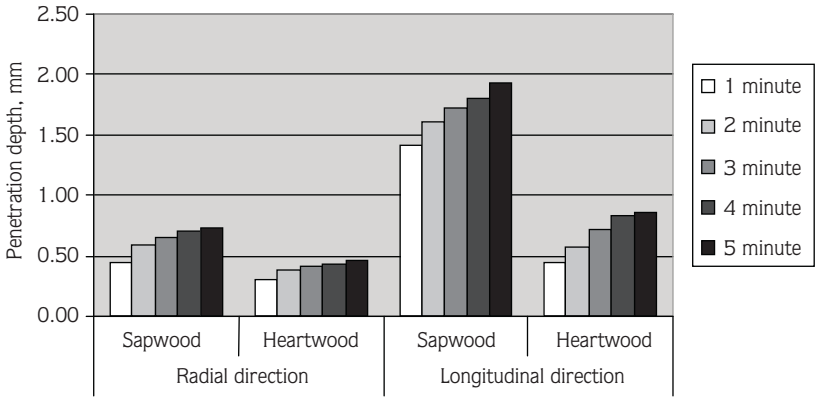

Figure 17. Longitudinal and radial penetration depth of safranine solution.

physical barrier for the mass flow of liquid (Wirspa and Libby, 1950). Above the fiber saturation point, wood can still take up water by absorption or capillary action until the cell cavities are filled with liquid water (Browning, 1963); therefore, liquid penetration in wood depends upon the sample moisture content. The moisture content of this species was 7.70%.

In the radial direction, ray cells are joined together to form a capillary structure that allows a pathway for safranine solution impregnation. Liquid can diffuse from one ray cell to the adjacent cells through pits (Figure 18). It has been reported that ray parenchyma cells are important channels for radial flow in some species (Usta and Hale, 2003). Safranine solution input may vary due to the ray parenchyma's diameter, length, end-wall pitting, and lateral wall pitting. To clarify the penetration depth variations, this experimental result was compared with the result reported by Ahmed et al. (2007). They reported that the radial flow depth of safranine solution after 4 min of impregnation was about 84.19 μm by ray parenchyma at the 23.27% wood moisture level; however, in the present experiment we observed a penetration depth of about 572 μm. This outcome can be explained by the moisture content, ray cell lumen diameter, end-wall pit number, end-wall pit diameter, and ray cell length differences between the 2 species. We measured the cross sectional areas of the ellipsoid ray parenchyma of *Populus tomentiglandulosa* and *Samanea saman*, which were about 187.35 and 423.59 μm^2, ray cell length was 63.32 and 127.41 μm, number of end-wall pit ray parenchyma was 9 and 5, and end-wall pit diameter was 1.15 and 2.81 μm, respectively. In both sapwood and heartwood, longer and narrower rays with wider openings through the end-wall pit could make safranine solution encounter fewer obstacles while flowing into the cell lumen. Another comparison was made from the results obtained by Ahmed and Chun (2007) in a diffuse porous wood species, *Gmelina arborea*. The presence of a smaller end-wall pit diameter (1.15) and a shorter compound ray parenchyma (body ray cell: 80.28 μm; marginal: 36.60 μm) might result in less radial penetration in *Gmelina arborea* than was observed in the present study's wood species.

The formation of deposits can subsequently reduce the permeability of heartwood (Kumar and Dobriyal, 1993). Gum deposition was observed in the heartwood vessels of *Samanea saman* and was responsible for the lower permeability of heartwood as compared with sapwood. In addition, the longitudinal penetration of liquid is dependent on size, distribution, and condition of the vessels (Bao et al., 1999). In *Populus tomentiglandulosa* and *Samanea saman* vessels per square millimeter was 95.36 and 4.20, vessel length was 583.30 and 263.52 μm, vessel diameter was 62.69 and 145.25 μm, fiber length was 1087.68 and 707.96 μm, and fiber diameter was 13.96 and 18.65 μm, respectively. Numerous long vessels with smaller

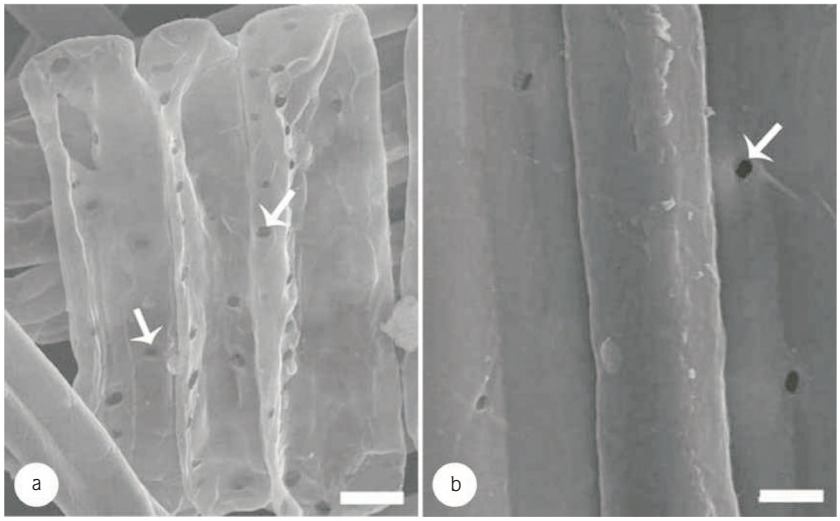

Figure 18. Ray parenchyma (a) and fiber (b) of *Samanea saman* observed under FE-SEM. Arrow shows pits. Scale bar in a = 10 μm; in b = 3 μm.

diameters and longer fibers could be responsible for the higher permeability of *Populus tomentiglandulosa* than that of *Samanea saman*. Liquid penetration data used for this comparison was obtained from the report by Choi et al. (2007).

Except vessel and wood fiber, axial parenchyma, and vascular or vascicentric tracheids can play an important role in liquid penetration in wood. It is reported that vascicentric tracheids can also function as a communication mechanism between the intervessel fluid transports (Wheeler and Thomas, 1981). Air present in cell lumina is the main obstacle to rapid penetration of liquid (Maass, 1953). This phenomenon was also observed in sapwood fibers of *Samanea saman* and is shown in Figure 19. Removal of air from wood void structure can improve liquid penetration (Stamn, 1953). When penetration is allowed from both sides of a woodchip, the backpressure of trapped air becomes compressed by capillary forces that immediately check the penetration. Air trapped in the capillaries (Figure 19) reduced the safranine solution penetration. In this case, pressure impregnation of liquid is effective (Chong et al., 2007). Moreover, Siau (1971) reported that the prime factors responsible for governing liquid flow are the amount of pressure, fluid viscosity, solvent contact angle, wood pore radius, and wood capillary length. Unless the externally applied pressure exceeds this flow opposing pressure, penetration cannot proceed further. Thus, pores of various radiuses are distributed throughout the wood specimen; the extent of and rate of penetration is directly related to the magnitude of the applied pressure.

Ray parenchyma forms a capillary tube by interconnecting with end-wall pitting. Safranine solution formed meniscus while passing through this capillary (Figure 20). This kind of structure was also observed and described by Chun and Ahmed (2006), and Choi et al. (2007). Measuring the radius of ray parenchyma capillary a as 6.2 μm and capillary b as 5.8 μm, the surface tension of safranine solution at 24 °C was 36.1 dynes cm^{-1}, the contact angle of the wetting phase (safranine solution) was 31.3° ± 6.35° (range: 21.8°-39.2°), and capillary pressure was 0.10 bar and 0.11 bar, respectively,

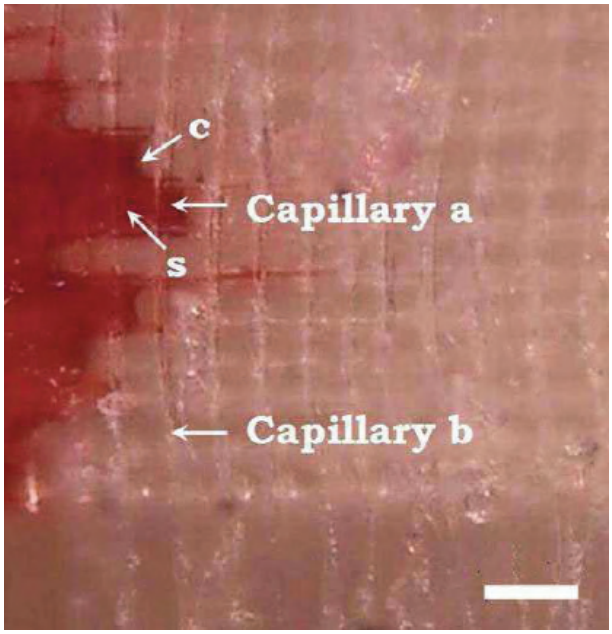

Figure 20. Meniscus observed in ray parenchyma of *Samanea saman*. c: curved air-safranine meniscus. s: Safranine solution. Scale bar = 25 μm.

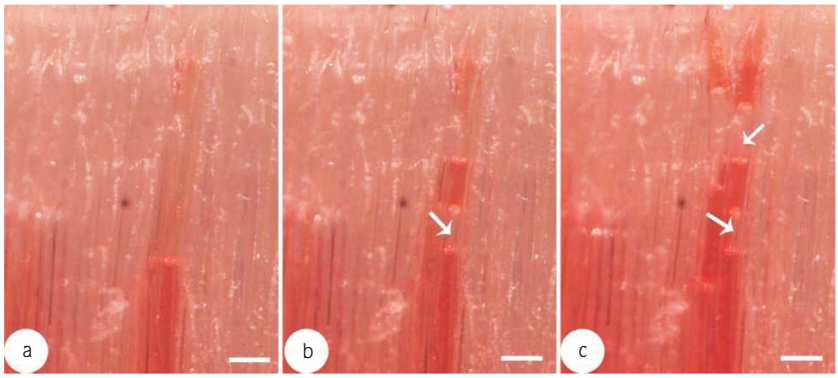

Figure 19. Gradual trapping of air in sapwood fiber of *Samanea saman*. a: After 1 min of safranine solution penetration. b: After 2 min of safranine solution penetration. c: After 3 min of safranine solution penetration. Arrow shows air trapped in cell lumen. Scale bars = 25 μm.

according to the Young-Laplace equation for a spherical meniscus in a cylindrical pore:

$$Pc = (2 \gamma \cos \theta)/r \quad (4)$$

where Pc is capillary pressure, γ is surface tension, θ is contact angle (a measure of wettability), and r is capillary radius. From the above equation it is clear that lumen diameter is inversely related to capillary pressure; therefore, wood fiber should have higher capillary pressure and thus higher penetration depth. Nonetheless, vessels were the primary avenue for safranine solution penetration. The anatomical structures of vessels and wood fiber are responsible for this phenomenon. Pits present in vessels or in wood fiber play an important role in trapping air inside the cell lumen. Because of numerous intervessel pits, lumen diameter and end-to-end connection with other vessels through the perforation plate makes the vessels more permeable than wood fiber.

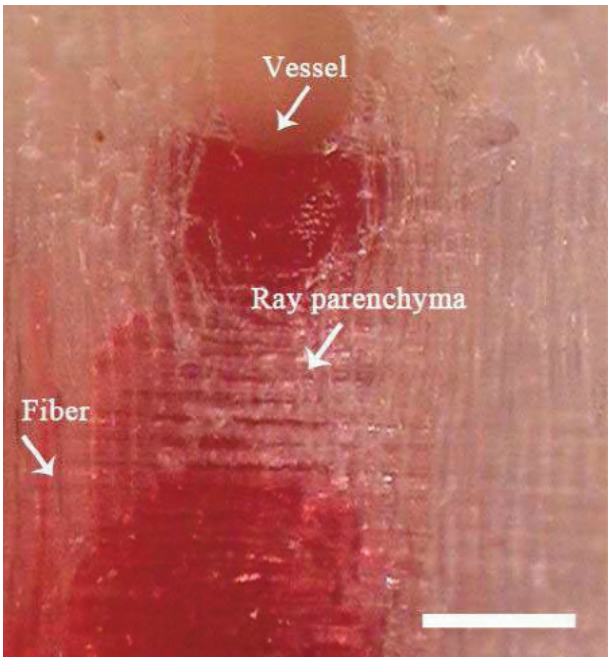

Figure 21. Safranine solution penetration in vessel and its surrounding cells. Scale bar = 100 μm.

Fibers present around the vessels conducted more safranine solution than those not associated with the vessels (Figure 21). It is assumed that trapped air in the lumen of wood fibers present around the vessels can easily bypass the air through pits. This non-steady state safranine solution flow depended upon different anatomical features as well as safranine solution characteristics. For example, the capillary invasion in a rough cell lumen surface better reflects the reality, since an absolute smooth surface does not exist; therefore, it would be very difficult, beyond that the lack of symmetry of the walls confers to the interface an asymmetrical appearance. Yet, a visual evaluation could be adequate. Note in Figure 20 that the curvature differences during penetration, which may have been caused by irregularities in the cell walls, in which the safranine solution had a very low speed due to the non-slip condition and remained motionless in some points of the surface, assumed the aspect of a real wet wall.

At the beginning, the safranine solution flow rate was high and then gradually declined in the both radial and longitudinal directions. It is thought that this phenomenon was due to the increasing probability of pore blockage within the flow path as flow path length increased. In both directions, the results show that the decrease in liquid flow was uneven. We can conclude from this result that liquid flowing in a radial or longitudinal direction followed a go-stop-go cycle until the capillary pressure of the safranine solution created by the cell lumen was equal to the pressure of air above the air-safranine solution interface. In this case, penetration was likely to be stopped.

Acknowledgements

This study was supported by the Korean Institute of Environmental Science and Technology and the Institute of Forest Science, Kangwon National University, Republic of Korea.

References

Ahmed, S.A. and S.K. Chun. 2007. Descriptions of the wood anatomy and safranine impregnation in *Gmelina arborea* Roxb. from Bangladesh. J. Korea Furnit. Soc. 18: 100-105.

Ahmed, S.A., S.N. Chae and S.K. Chun. 2007. Radial penetration of safranine in *Populus tomentiglandulosa* T. Lee. J. Korea Furnit. Soc. 18: 243-247.

Baas, P. and X. Zhang. 1986. Wood anatomy of tree and shrubs form China. I. Oleaceae. IAWA Bull. n. s. 4: 141-159.

Banks, W.B. 1981. Addressing the problem of non-steady state liquid flow in wood. Wood Sci. Technol. 15: 171-177.

Bao, F., J. Lu and S. Avramidis. 1999. On the permeability of main wood species in China. Holzforchung. 53: 350-354.

Bolton, A.J. 1988. A re-examination of some deviations from Darcy's Law in coniferous wood. Wood Sci. Technol. 22: 311-322.

Browning, B.L. 1963. The Chemistry of Wood. Interscience Publishers, New York.

Choi, I.S., S.A. Ahmed and S.K. Chun. 2007. Longitudinal flow path of safranine in *Populus tomentiglandulosa* T. Lee. J. Korea Furnit. Soc. 18: 161-165.

Chong, S.H, S.A. Ahmed and S.K. Chun. 2007. Pressure effect on safranine penetration in some hardwood species. J. Korea Furnit. Soc. 18: 111-119.

Chun, S.K. and S.A. Ahmed. 2006. Permeability and meniscus phenomenon in four Korean softwood species. For. Stud. China. 8: 56-60.

Comstock, G.L. 1968. Relationship between permeability of green and dry Eastern hemlock. Forest Prod. J. 18: 20-23.

Essiamah, S. and W. Eschrich. 1985. Changes of starch content in the storage tissue of deciduous trees during winter and spring. IAWA Bull. n.s. 6: 97-106.

Exley, R.R., B.A. Meylan and B.G. Butterfield. 1977. A technique for obtaining clear cut surfaces on wood samples prepared for the scanning electron microscope. J. Microscopy. 110: 75-78.

Fujii, T., S.J. Lee, N. Kuroda and Y. Suzuki. 2001. Conductive function of intervessel pits through a growth ring boundary of *Machilus thunbergii*. IAWA J. 22: 1-14.

Hansamann, C., W. Gindl, R. Wimmer and A. Teischinger. 2002. Permeability of wood: A review. Wood Res. Drevarsky Vysk. 47: 1-16.

IAWA Committee. 1989. IAWA list of microscopic features of hardwood identification. IAWA Bull. n.s. 10(3).

Kamke, F.A. and J.N. Lee. 2007. Adhesive penetration in wood- A review. Wood Fiber Sci. 39: 205-220.

Kumar, S. and P.B. Dobriyal. 1993. Penetration indices of hardwoods: a quantitative approach to define treatability. Wood Fiber Sci. 25: 192-197.

Leal, S., V.B. Sousa and H. Pereira. 2007. Radial variation of vessel size and distribution in cork oak wood (*Quercus suber* L.). Wood Sci. Technol. 41: 339-350.

Maass, O. 1953. The problem of penetration. Pulp and Paper Magazine of Canada. 54: 98-103.

Owoyemi, J.M. and J.O. Kayode. 2008. Effect of incision on preservative capacity of *Gmelina arborea* wood. Biotech. 7: 351-353.

Sano, Y. 2004. Intervascular pitting across the annual ring boundary in *Betula platyphylla* var. *japonica* and *Fraxinus mandshurica* var. *japonica*. IAWA J. 25: 129-140.

Siau, J.F. 1971. Flow in Wood. Syracuse University Press, London.

Stamn, A.J. 1953. Diffusion and penetration mechanism of liquids into wood. Pulp and Paper Magazine of Canada. 54: 54-63.

Thomas, R.J. 1976. Anatomical features affecting liquid penetrabi1ity in three hardwood species. Wood Fiber. 7: 256-263.

Usta, I. and M.D. Hale. 2003. Radial permeability of Sitka Spruce as affected by wood structure. IAWA J. 24: 197-204.

Virta, J., S. Koponen and I. Absetz. 2006. Modeling moisture distribution in wooden cladding board as a result of short-term single-sided water soaking. Building Environ. 41: 1593-1599.

Watanabe, U., Y. Imamura and I. Iida. 1998. Liquid penetration of precompressed wood VI: Anatomical characterization of pit fractures. J. Wood Sci. 44: 158-162.

Wheeler, E.A. and R.J. Thomas. 1981. Ultrastructure characteristics of mature wood of southern red oak (*Quercus falcata* Michx.) and white oak (*Quercus alba* L.). Wood Fiber. 13: 169-81.

Wirspa, V.J. and C.E. Libby. 1950. Penetration of neutral sulphite cooking liquors into yellow birch wood. Tappi. 33: 225-231.